applied optics

Speckle-based structured light shift-keying for non-line-of-sight optical communication

Purnesh Singh Badavath,[1] Venugopal Raskatla,[1,2] T. Pradeep Chakravarthy,[3] and Vijay Kumar[1,*]

[1]Department of Physics, National Institute of Technology Warangal, Warangal, Telangana 506004, India
[2]Current address: Optoelectronics Research Centre and Centre for Photonic Metamaterials, University of Southampton, Highfield, Southampton SO17 1BJ, UK
[3]School of Physics, University of Hyderabad, Hyderabad, Telangana 500046, India
*vijay@nitw.ac.in

Received 2 February 2023; revised 12 April 2023; accepted 12 April 2023; posted 12 April 2023; published 3 May 2023

We report an experimental proof of concept for speckle-based one-to-three non-line-of-sight (NLOS) free space optical (FSO) communication channels employing structured light shift-keying. A 3-bit gray image of resolution 100 × 100 pixels is encoded in Laguerre–Gaussian or Hermite–Gaussian beams and decoded using their respective intensity speckle patterns via trained 1D convolutional neural network. We have achieved an average classification accuracy of 96% and 93% using LG_{ml} and HG_{pq} beams, respectively, among all three channels. It demonstrates the directional independence and broadcasting capability of speckle-based decoding (SBD) in FSO communication using structured light. Further, we have extended the study from 2D to 1D SBD in one-to-three NLOS FSO communication channels to decrease the computational cost and to emphasize the importance of the 1D SBD approach.

https://doi.org/10.1364/AO.486919

1. INTRODUCTION

With the rapid advances in technology, we are moving towards an artificial intelligence (AI) driven society, which has led to a massive increment in network traffic [1]. To avoid the capacity crunch, many attempts have been made to develop networks that provide substantially higher transmission capacity and much lower latency. Over the past decade, structured light beams have emerged as a viable candidate for increasing spectral efficiency in free space and fiber optical communication links. Structured light with tailored complex amplitude or polarization, employed in space-division multiplexing (SDM), has surged the data transmission rates up to terabit/s and petabit/s by utilizing its spatial degree of freedom [2–5]. The prominent advantage of these beams is that almost any complete orthogonal modal basis set can be utilized for encoding information in optical communication links by efficiently combining different fundamental modes. Various modal basis sets such as Laguerre–Gaussian (LG_{ml}) and their superposition beams, Hermite–Gaussian (HG_{pq}), and Bessel–Gaussian beams have been experimentally demonstrated in free space or fiber-based communication links [6–8].

In general, structured light has been exploited in various communication systems but the pioneering work was focused on on-axis or line-of-sight (LOS) communication. On-axis or one-to-one communication channels are established with structured light in different encoding schemes using traditional interference and diffraction techniques [9–11]. Recently, orbital angular momentum (OAM)-based non-LOS (NLOS) has been reported while demonstrating the broadcasting capability of OAM beams [12]. Although structured light increases the channel capacity by manyfold, its uses are limited by various technological challenges. The optical communication channel's information transfer rate is determined by the frame rate at which the structured light beams are generated. The most popular way to generate them is by using spatial light modulator (SLM) and digital micromirror devices (DMD) , but the commercially available SLM and DMD have very low frame rates, thus limiting the bandwidth.

In NLOS communication, scattering effects and the increased signal-to-noise ratio lead to high cross talk among structured light beams. In the case of speckle pattern classification using AI-based methods, the cross talk among beams off-axis is much higher than that on-axis. The misclassification or the cross talk among structured light beams is because of the decrease in signal intensity and increase in noise at off-axis receivers. In recent years, rapid advances in parallel computing and low-cost computing hardware have made big data modeling possible. With this development, AI has empowered a wide range of aspects of optical communication by overcoming technological challenges. Structured-light-employed communication links have been augmented and elevated with AI-based decoding techniques for the past decade [13–16]. Making

the most of this opportunity, optical engineers/researchers have demonstrated structured light recognition and (de)multiplexing using machine learning even under the presence of noise in space, underwater, and in turbulence [13,17]. Machine learning models have reduced the complexity of handling sensitive and bulky optical instruments and boosted performance by increasing noise tolerance. Such AI-based decoding schemes have reduced the intricacy of the receivers and decreased the decoding time. Because of the decreased decoding time, AI-based decoding techniques have laid the foundation for real-time FSO communication using structured light [18,19]. Recently, the speckle-based decoding (SBD) technique has been introduced in FSO communication channels and established an "alignment-free" decoding technique [20–28]. SBD is proven to identify the dislocations present in employed structured light using far-field intensity speckle patterns rather than the direct beam cross-sectional intensity profile.

Traditional AI-based demultiplexing method need a camera preferably with a larger imaging area to capture higher-order beams, which are comparatively larger in size than lower-order beams, thus limiting AI-based demultiplexing techniques to lower-order modes. The proposed model of the speckle-based demultiplexing method has an advantage over traditional AI-based demultiplexing methods. The speckle-based demultiplexing method can identify structured light even by capturing a small part of the speckle field even in a high-noise environment [27]. This proves that the proposed demultiplexing method does not need a large imaging area camera. Commercially available cameras (Thorlab's CMOS CS235CU) are good enough for the present task. For 1D speckle-based demultiplexing, 1D cameras can be a cost-effective alternative. The key takeaway of this technique is that a small portion of the speckle field having enough speckle grains is adequate for the recognition of structured light.

Vizualizing lower-dimensional data (1D) in higher dimensions (2D or 3D) gives us deeper insight to understand lower-dimentional data, which makes complex features easily interpretable in higher dimensions. Such data visualizations are very popular in health monitoring systems such as electrocardiograms (ECGs) [29,30], cardiovascular disease analysis [31], and driving event analysis [32].

In the proposed method of structured light demultiplexing in NLOS, classification of structured light beams has been achieved by employing 2D speckle pattern images and 1D speckle arrays. Rather than projecting the lower dimentions to higher dimensions, we have reduced the dimentionality of the raw data (2D to 1D) to achieve classification accuracy. In the 1D speckle-based demultiplexing method, the 1D speckle array (1×20 pixels) has less than one-by-thousandth of 2D speckle data (1200×1920 pixels). To the best of our knowledge, the proposed method using 1D information (1D speckle array) and 2D information (2D speckle pattern image) in structured light NLOS communication is the first to be reported. In this paper, we extend one-to-one communication [25,26] to one-to-many NLOS communication channels utilizing the speckle-based information broadcasting capability of structured light beams.

We have used eight different LG_{ml} or HG_{pq} beams to encode a 3-bit gray image of 100×100 pixel resolution. A 1D convolutional neural network (CNN) is trained on the speckle features of 2D intensity speckle images and deployed in one-to-three NLOS FSO communication channels to decode the encoded information. The trained network effectively classifies LG_{ml} and HG_{pq} beams with average classification accuracies of 96% and 93%, respectively, in 3-bit NLOS FSO communication channel links. Extending this study from 2D to 1D SBD, we have trained and tested 1D CNN to classify structured light beams using 1D speckle information and deployed it in the established 3-bit NLOS communication channel. Finally, we also explored our approach of 2D and 1D SBD schemes to classify intensity degenerate LG_{ml} beams to exploit the advantage of their full modal spectrum.

2. STRUCTURED LIGHT

Structured light has played a vital role in different research areas because of its flexibility in tailoring its phase and amplitude according to the application. In a family of structured light beams, LG_{ml} beams carry OAM and have been of great potential in communication. LG_{ml} beams can be tailored by using the azimuthal index (l) and radial index (m). The complex amplitude of the LG_{ml} beam is given by

$$\mathrm{LG}_{m,l}(r,\phi,z) = A_{l,m}\left[\frac{W_0}{W(z)}\right]\left(\frac{\rho}{W(z)}\right)^{l} L_m^l\left(\frac{2\rho^2}{W^2(z)}\right) \times \exp\left(-\frac{\rho^2}{W^2(z)}\right) \times \exp\left[-ikz - ik\frac{\rho^2}{2R(z)} \mp il\phi + i(l+2m+1)\zeta(z)\right].$$

Here L_m^l, $W(z)$, and $R(z)$ represent the Laguerre polynomial, beam width, and radius of curvature, respectively. $LG_{o,\pm l}$ beams have identical intensity profiles for a given value of l, and are called intensity degenerate beams. Decoding the information in intensity generate beams is impossible just by using a cross-sectional plane of their intensity profiles. Researchers introduce astigmatic transformation to break the degeneracy [24,33,34]. Information encoding using OAM beams can effectively address spectral efficiency issues by utilizing its orthogonal property.

Theoretically, infinite m values can be utilized to increase the number of communication channels in a given bandwidth per l value and decode the encoded beams with minimal cross talk among channels. But in this work, we restrict ourselves to $m = 0$ and utilize both sides of the OAM spectrum ($\pm l$). Not only OAM beams but also non-OAM beams have contributed to establishing FSO communication links.

In this work, we have also explored HG_{pq} beams to establish FSO communication links. The complex amplitudes of HG_{pq} beams are expressed by the equation

$$\mathrm{HG}_{p,q}(x,y,z) = A_o\left[\frac{W_0}{W(z)}\right] H_p\left(\frac{\sqrt{2}x}{W(z)}\right) H_q\left(\frac{\sqrt{2}y}{W(z)}\right) \times \exp\left[-ikz - ik\frac{x^2+y^2}{2R(z)} + i(p+q+1)\zeta(z)\right],$$

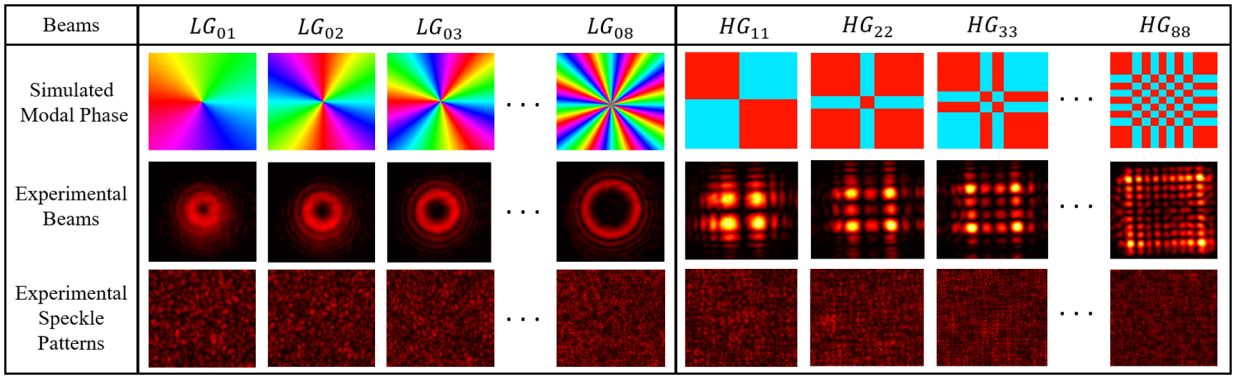

Fig. 1. Experimentally generated structured light beams and their corresponding speckles.

where A_o represents constant amplitude. H_p and H_q are Hermite polynomials of orders p and q, and indices p and q give the number of nodal lines along y and x axes in the beam cross section, respectively. HG_{pq} beams also possess orthogonality properties, which is a potent property to increase the spectral efficiency of a communication link. Experimentally generated LG_{ml} and HG_{pq} beams and their corresponding speckle patterns are shown in Fig. 1.

3. EXPERIMENTAL SETUP

An experimental setup for one-to-three NLOS FSO communication channel links is established and tested. A phase-only SLM is illuminated using a 3 mW He–Ne laser. To realize shift-keying, structured light beams are generated by updating the corresponding fork pattern holograms onto the SLM. Speckle patterns are generated by passing the beams through a rotating ground glass. The ground glass is connected to a 12 V DC motor with a speed controller. The RPM of the ground glass is adjusted to be less than the camera exposure time (194 μs) to avoid blurring speckles and to capture speckles with good contrast. The ground glass is rotated to capture multiple intensity speckle pattern images to train the CNN model.

The speckle pattern generated depends upon the beam size and the ground glass. A fixed ground glass with varying beam sizes will affect the speckle size, but not speckle pattern distribution. Speckle size is inversely proportional to beam size. Even though beam size affects speckle size, machine learning algorithms learn from the multiple complex features representing speckle distribution to classify structured light beams [21]. The change in beam size does not affect the machine learning model's classification accuracy as long as speckles are captured with good contrast.

Speckle pattern images are captured using a CMOS camera (Thorlab's CMOS CS235CU) directly without any additional lenses or filters at the rate of one image/s. The captured speckle images has a resolution of 1200 × 1920 pixels at three different positions [$C_0(0°)$, $C_{+15}(15°)$, and $C_{-15}(-15°)$] within the horizontal beam axis plane, maintaining the radial distance of 26 cm from the ground glass plane as shown in Fig. 2. The captured intensity speckle patterns are used to decode the encoded information using the SBD technique. The 3-bit structured light shift-keying is achieved using LG_{ml} beams with

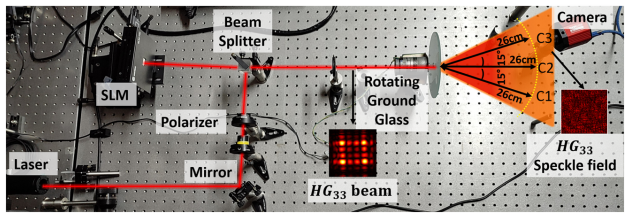

Fig. 2. Experimental setup for speckle-based structured light shift-keying for one-to-three NLOS FSO communication channels.

$m = 0$ and $l = [+1, +8]$, excluding $l = 0$ or HG_{pq} beams with $p = q = [1, 8]$.

We considered eight LG beams for 3-bit structured light shift-keying. For each beam, we captured 500 images at each receiver position. A total of 4000 (500 × 8) speckle images were captered for eight LG beams per receiver. At three different receiver positions [$C_0(0°)$, $C_{+15}(15°)$, and $C_{-15}(-15°)$], we captured 12,000 (4000 × 3) speckle images for the LG_{ml} beam data set. The same number of images were captured for HG beams. For 1D SBD, an array of size only 1 × 1920 pixels was mapped from the captured images of size 1200 × 1920 pixel resolution. First, the features were extracted from speckle images or arrays via a wavelet scattering network (WSN), and the extracted features were fed to train 1D CNN for beam classification.

4. DEEP LEARNING ANALYSIS

A. Wavelet Scattering Transform

The wavelet scattering transform is a well-known feature extraction technique that has been used to generate scattering coefficients to train machine learning and deep learning neural networks. The wavelet scattering transform processes data and extracts scattering coefficients at different frequencies. Scattering coefficients represent data much better in frequency and time domains than their raw representation [35]. As WSN processes the data at different frequencies with different values of scaling factors, it provides us with rich and enhanced data interpretability through scattering coefficients. The Morlet wavelet in the WSN goes through scaling and shifting while striding over the input signal's frequency and intensity. At each scaling value, the network shifts the wavelet through the entire

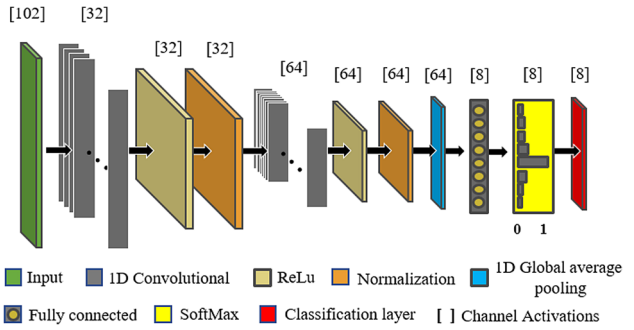

Fig. 3. 1D CNN architecture and corresponding channel activations.

spatial or time domain of the data and extracts the scattering coefficients at that frequency.

To capture scattering coefficients at higher frequencies, the scaling factor goes down and extracts the scattering coefficients at higher frequency domains or at smaller intervals of time. Scattering coefficients extracted by the wavelet scattering transform correspond to multi-resolution data interpretation in frequency and time domains. This results in the accurate classification of signals or images with high precision in machine learning and deep learning networks [23,36–38]. At each level of the scattering network, the input data go through convolution, non-linearity, and averaging operations. The scattering coefficients for images of size 512 × 512 pixels (cropped from the original images of 1200 × 1920 pixels) and cross-line arrays of size 1 × 1920 pixels were extracted and fed to the 1D CNN network to train.

B. 1D Convolutional Neural Network

1D CNN has a compact and simple structure and can be trained on both 2D images and 1D arrays. 1D CNN has advantages in signal processing over other deep learning neural networks. It has become a state-of-the-art technique for classifying signals of various kinds with minimal computational resources. Using 1D CNN over conventional 2D CNN gives us the advantages of fewer training data and computational resources and less training time. Day-to-day life involves 1D signals as much as 2D signals such as high-power circuitry, acoustics, damage detection in structures, vibrations, arrhythmia detection in ECGs [39–41], etc. The designed architecture of our 1D CNN is shown in Fig. 3. We have used a sequential input layer that can accept the scattering coefficients of images and crossline arrays without modifying 1D CNN architecture. To decrease the computational load and to overcome the gradient vanishing and the explosion issue at the same time, we have inculcated only two 1D convolutional layers with 32 and 64 filters in the 1D CNN architecture.

Each 1D convolutional layer is followed by ReLu and normalization layers. The ReLu layer uses a non-linear activation function to threshold the values convolved from the convolutional layer. The ReLu layer is followed by the normalization layer, which independently normalizes input elements by calculating the mean and variance for the possible dimensions for every observation. After the two sets of 1D convolutional, ReLu, and normalization layers, a 1D global averaging pooling layer is used for subsampling by giving the average over the time or spatial domain, followed by a fully connected layer for the required number of classes followed by a SoftMax layer and classification layer. At the output layer, cross-entropy is minimized by using the Adam optimizer. The defined hyperparameters have a constant learning rate of 0.0001, a mini-batch of size 120, and 150 epochs with the necessary casual padding and stride 1. The hypermeters are optimized manually as they are case specific. The designed 1D CNN is always trained on 80% of collected data and tested on the remaining unseen 20% of data. The designed 1D CNN architecture gives high classification accuracy on fewer training data with only 11.4 thousand learnable parameters.

5. 3-BIT NLOS STRUCTURED LIGHT SHIFT-KEYING

A. 2D Speckle-Based Decoding

A proof of concept to demonstrate NLOS optical communication through structured light shift-keying for a 3-bit image is carried out using beams with $m = 0$ and $l = [+1 \text{ to } +8]$, as well as using HG_{pq} beams with $p = q = [1 \text{ to } 8]$. Figure 4 shows its experimental realization. The eight gray levels of a 3-bit image of 100 × 100 pixels are encoded in the eight beams (LG_{ml} or HG_{pq}) via SLM. The information is encoded in structured light beams, which are passed through the ground glass. The far-field intensity speckles are collected at a beam on-axis position (C_0 channel) and at two beam off-axis positions (C_{+15} and C_{-15} channels) using a CMOS camera. A portion of 512 × 512 pixels is cropped from the originally captured image of 1200 × 1920 pixels. The features are extracted from the cropped images of all channels using WSN and fed to 1D CNN for training and testing.

1D CNN is always trained and tested on 80% and 20% of data, respectively. For 3-bit NLOS FSO communication, we achieve a classification accuracy of >99%(96%) at the on-axis channel C_0 and 95%(92%) and 93%(93%) on the beam off-axis channels C_{+15} and C_{-15}, respectively, using $\mathrm{LG}_{ml}(\mathrm{HG}_{pq})$ beams as noted in Table 1. In 2D speckle-based demultiplexing, the trained 1D CNN performs quite similarly in classifying LG and HG beams among all three channels.

The accuracy achieved by the CNN model in 2D SBD tends to decrease as the off-axis range increases. The off-axis range of the NLOS communication channel is inversely proportional to the grit size of the ground glass. Some diffusers have a range of up to ±25° depending upon the grit size, which will increase the range of the NLOS communication. The range of off-axis (±15°) and the radial distance (26 cm) in NLOS communication are chosen appropriately to capture the speckle field with good intensity and contrast.

B. 1D Speckle-Based Decoding

In this section, we report information decoding by using only the 1D array in contrast to the previous section where we used 2D images for information decoding. This time, randomly mapped 1D crossline arrays across the originally captured intensity speckle images are used to extract the features and train

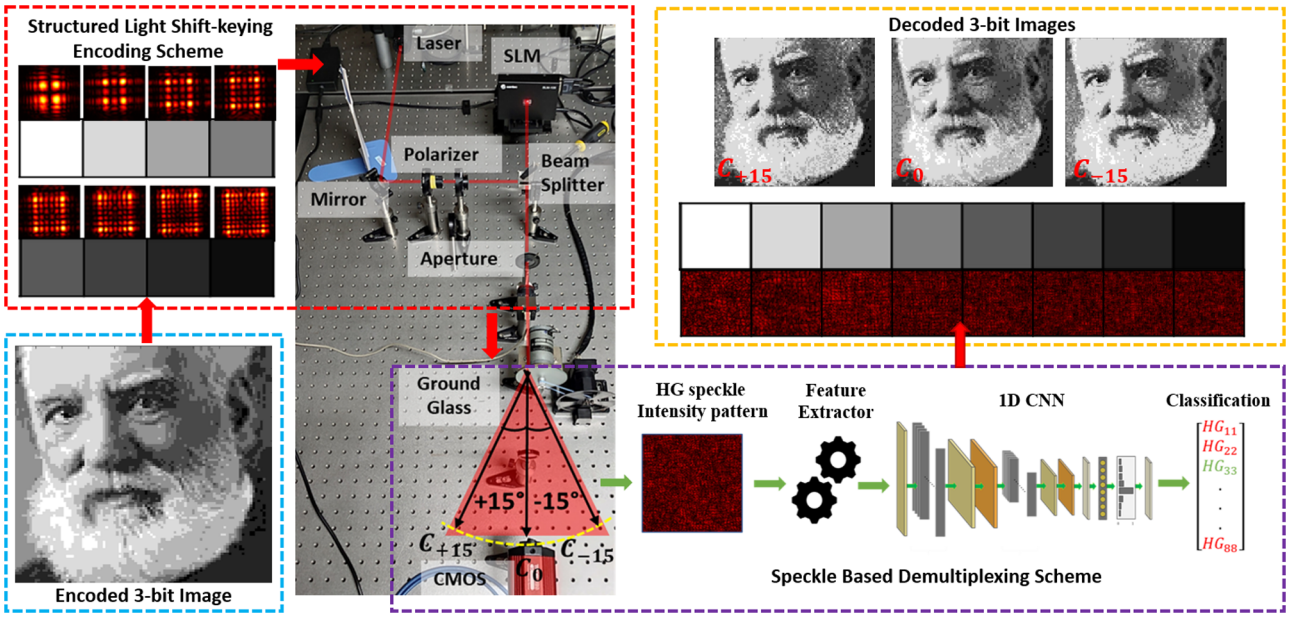

Fig. 4. Speckle-based structured light shift-keying for NLOS optical communication using the HG_{pq} beam. The blue box shows the encoded image. The red box shows the encoded scheme and its experimental realization. The purple box shows the 2D SBD. The yellow box shows the decoding scheme and the decoded images at channels C_{+15}, C_0, and C_{-15}.

Table 1. Decoding Accuracies for 3-bit NLOS FSO Communication Using SBD

	Accuracies in %					
	HG Beams ($HG_{11} - HG_{88}$)		LG Beams ($LG_{01} - LG_{08}$)		LG Beams ($LG_{0-8} - LG_{0+8}$)	
	2D-SBD	1D-SBD	2D-SBD	1D-SBD	2D-SBD	1D-SBD
C_{+15}	92	69	95	49	79	40
C_0	96	72	99	72	96	61
C_{-15}	93	49	93	35	76	22

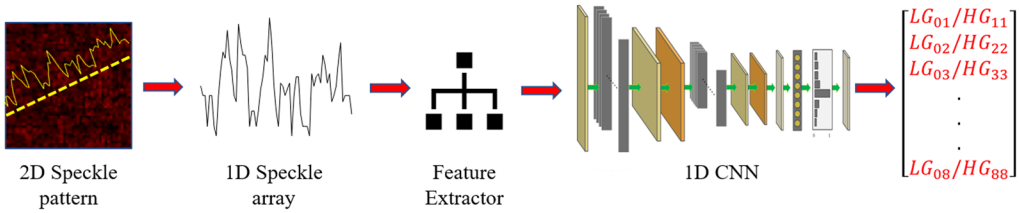

Fig. 5. Structured light shift-keying employing 1D SBD in NLOS FSO communication.

the 1D CNN. Mapping a 1D array randomly across any direction from the captured speckle pattern proves the directional independence of the modal information in intensity speckle patterns. The schematic flow of the data in 1D SBD is shown in Fig. 5. The maximum classification accuracy of 72% is achieved at the on-axis channel C_0 using both LG_{ml} and HG_{pq} beams. The accuracies at the off-axis channels (C_{+15} and C_{-15}) are not promising, but HG_{pq} beams perform significantly better than LG_{ml} beams (Table 1).

In 1D speckle-based demultiplexing, HG beams achieve higher classification accuracy than LG beams in off-axis channels. 1D speckle array features represent the HG beam more distinctively than LG. Off-axis, signal intensity drops and noise increases, as HG beams are much more distinct and robust than LG. CNN achieves higher classification accuracy for HG beams than LG beams at off-axis channels in 1D speckle-based demultiplexing. These accuracies can be improved by optimizing the encoding/decoding scheme and using a deep neural network for accurate classification.

6. NLOS CLASSIFICATION OF INTENSITY DEGENERATE LG_{ml} BEAMS

We further extend our analysis to intensity degenerate LG_{ml} beams with $m = 0$ and $l = [-8 \text{ to } +8]$, excluding $l = 0$. The 2D SBD technique adopted in Section 5.A. is followed for this class of data. For the case of 2D speckle images of the corresponding intensity degenerate beams, 1D CNN achieved classification accuracies of 79%, 96%, and 76% at C_{+15}, C_0,

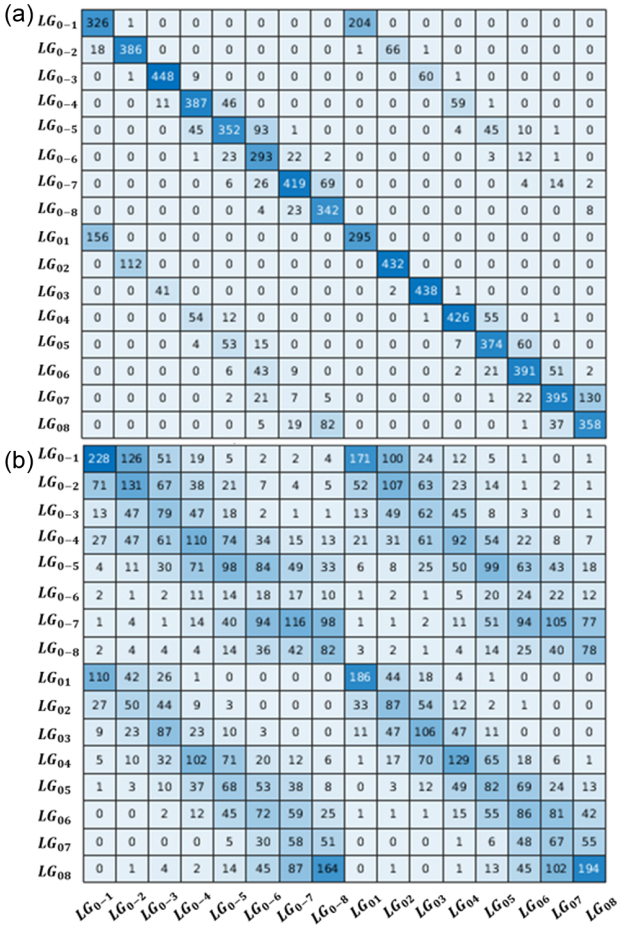

Fig. 6. Confusion matrix for channel C_{-15} employing (a) 2D SBD and (b) 1D SBD in intensity degenerate LG_{ml} beams.

and C_{-15} channels, respectively. Figure 6(a) shows the confusion matrix for the C_{-15} channel. It shows that free space propagation breaks the degeneracy of intensity degenerate beams. The confusion matrix in Fig. 5(a) exhibits less cross talk among adjacent beams and high cross talk among $\pm l$ beams for lower-order beams and exhibits low cross talk among $\pm l$ beams and high cross talk among the adjacent beams for higher-order beams. Similar cross talk is present in the C_{+15} channel as well.

The 2D SBD of intensity degenerate beams in NLOS FSO communication is also extended to 1D SBD. Following the methods described in Section 5.B, 1D crossline arrays randomly picked from 2D speckle images are used to classify intensity degenerate beams. The trained 1D CNN achieves classification accuracies of 40%, 61%, and 22% on channels C_{+15}, C_0, and C_{-15}, respectively. The cross talk among the intensity degenerate LG_{ml} beams in channel C_{-15} is shown in Fig. 6(b).

7. CONCLUSIONS

A proof of concept for NLOS FSO communication is demonstrated by employing structured light shift-keying. The proposed idea of one-to-"n" communication channel links using speckle-based communication can multiply the advantage by "n" times in the established NLOS FSO communication. In 2D SBD, a small portion of the entire speckle is sufficient to classify the structured light in contrast to a full beam intensity image. The SBD also makes the employed communication channel link alignment independent.

The proposed model of speckle-based demultiplexing can impact FSO NLOS communication by increasing the information transfer of the communication channel by $1 \times n$ receivers. Realizing the potential of structured light (OAM) beams in increasing spectral efficiency could add advantages to the NLOS communication channel. The proposed NLOS communication can be realized practically in the near future as a short-range communication channel, for example, LiFi. Employing a speckle-based demultiplexing method in the NLOS communication channel has a potential impact on reducing the computational load in demultiplexing the encoded information.

The 2D speckle-based demultiplexing technique has high fidelity and can be deployed in NLOS communication channels. The 1D speckle-based demultiplexing method uses only one-by-thousandth of the 2D speckle pattern image, which reduces the computational load drastically on deep learning algorithms. The proposed 1D speckle-based demultiplexing method can be realized with great feasibility, even in small-scale deployment, and with minimal computational resources. Both 2D and 1D speckle-based demultiplexings in FSO NLOS communication are practical solutions that can be implemented at a low cost, thereby enhancing their accessibility and potential impact.

Further research must be conducted on improving NLOS communication. Extensive research must be done on increasing the range and accuracies of NLOS off-axis communication channels. A detailed study has to be conducted on different preprocessing techniques to reduce the noise effects at off-axis channels while employing 1D and 2D speckle-based demultiplexing methods. The feature extraction techniques and the network used in this research are basic and have a compact structure. Further improvements can be made by opting for different feature extraction techniques and also by designing deep and effective neural networks.

Funding. Science and Engineering Research Board (SRG/2021/001375).

Acknowledgment. We acknowledge Prof. Nirmal K. V, University of Hyderabad, for allowing us to use his laboratory facility.

Disclosures. The authors declare no conflicts of interest.

Data availability. Data underlying the results presented in this paper are not publicly available at this time but may be obtained from the authors upon reasonable request.

REFERENCES

1. F. P. Guiomar, M. A. Fernandes, J. L. Nascimento, V. Rodrigues, and P. P. Monteiro, "Coherent free-space optical communications: opportunities and challenges," J. Lightwave Technol. **40**, 3173–3186 (2022).
2. H. Huang, G. Xie, Y. Yan, N. Ahmed, Y. Ren, Y. Yue, D. Rogawski, M. J. Willner, B. I. Erkmen, K. M. Birnbaum, S. J. Dolinar, M. P. J. Lavery, M. J. Padgett, M. Tur, and A. E. Willner, "100 Tbit/s free-space data link enabled by three-dimensional multiplexing of orbital angular momentum, polarization, and wavelength," Opt. Lett. **39**, 197–200 (2014).
3. G. Rademacher, B. J. Puttnam, R. S. Luís, T. A. Eriksson, N. K. Fontaine, M. Mazur, H. Chen, R. Ryf, D. T. Neilson, P. Sillard, F.

Achten, Y. Awaji, and H. Furukawa, "Peta-bit-per-second optical communications system using a standard cladding diameter 15-mode fiber," Nat. Commun. **12**, 4238 (2021).
4. B. J. Puttnam, R. S. Luis, G. Rademacher, L. Galdino, D. Lavery, T. A. Eriksson, Y. Awaji, H. Furukawa, P. Bayvel, and N. Wada, "0.61 Pb/s S, C, and L-band transmission in a 125 μm diameter 4-core fiber using a single wideband comb source," J. Lightwave Technol. **39**, 1027–1032 (2021).
5. A. E. Willner, X. Su, H. Zhou, A. Minoofar, Z. Zhao, R. Zhang, M. Tur, A. F. Molisch, D. Lee, and A. Almaiman, "High capacity terahertz communication systems based on multiple orbital-angular-momentum beams," J. Opt. **24**, 124002 (2022).
6. A. E. Willner, H. Huang, Y. Yan, Y. Ren, N. Ahmed, G. Xie, C. Bao, L. Li, Y. Cao, Z. Zhao, J. Wang, M. P. J. Lavery, M. Tur, S. Ramachandran, A. F. Molisch, N. Ashrafi, and S. Ashrafi, "Optical communications using orbital angular momentum beams," Adv. Opt. Photon. **7**, 66–106 (2015).
7. A. E. Willner and C. Liu, "Perspective on using multiple orbital-angular-momentum beams for enhanced capacity in free-space optical communication links," Nanophotonics **10**, 225–233 (2020).
8. M. Singh, M. H. Aly, and S. A. Abd El-Mottaleb, "6G enabling FSO communication system employing integrated PDM-OAM-OCDMA transmission: impact of weather conditions in India," Appl. Opt. **62**, 142–152 (2023).
9. J. C. Dainty, *Laser Speckle and Related Phenomena* (Springer, 1975), Vol. **9**.
10. J. M. Hickmann, E. J. S. Fonseca, W. C. Soares, and S. Chávez-Cerda, "Unveiling a truncated optical lattice associated with a triangular aperture using light's orbital angular momentum," Phys. Rev. Lett. **105**, 053904 (2010).
11. P. Ma, X. Liu, Q. Zhang, Q. Chen, J. Zeng, Y. Cai, Q. Zhan, and C. Liang, "Universal orbital angular momentum detection scheme for any vortex beam," Opt. Lett. **47**, 6037–6040 (2022).
12. Z. Liu, Y. Huang, H. Liu, and X. Chen, "Non-line-of-sight optical communication based on orbital angular momentum," Opt. Lett. **46**, 5112–5115 (2021).
13. M. Krenn, R. Fickler, M. Fink, J. Handsteiner, M. Malik, T. Scheidl, R. Ursin, and A. Zeilinger, "Communication with spatially modulated light through turbulent air across Vienna," New J. Phys. **16**, 113028 (2014).
14. M. Krenn, J. Handsteiner, M. Fink, R. Fickler, R. Ursin, M. Malik, and A. Zeilinger, "Twisted light transmission over 143 km," Proc. Natl. Acad. Sci. USA **113**, 13648–13653 (2016).
15. T. Doster and A. T. Watnik, "Machine learning approach to OAM beam demultiplexing via convolutional neural networks," Appl. Opt. **56**, 3386–3396 (2017).
16. L. R. Hofer, L. W. Jones, J. L. Goedert, and R. V. Dragone, "Hermite–Gaussian mode detection via convolution neural networks," J. Opt. Soc. Am. A **36**, 936–943 (2019).
17. Y. Na and D. K. Ko, "Adaptive demodulation by deep-learning-based identification of fractional orbital angular momentum modes with structural distortion due to atmospheric turbulence," Sci. Rep. **11**, 23505 (2021).
18. A. Bekerman, S. Froim, B. Hadad, and A. Bahabad, "Beam profiler network (BPNet): a deep learning approach to mode demultiplexing of Laguerre–Gaussian optical beams," Opt. Lett. **44**, 3629–3632 (2019).
19. H. Zhou, Y. Wang, X. Li, Z. Xu, X. Li, and L. Huang, "A deep learning approach for trustworthy high-fidelity computational holographic orbital angular momentum communication," Appl. Phys. Lett. **119**, 044104 (2021).
20. V. Raskatla and V. Kumar, "Deep learning assisted OAM modes demultiplexing," in *Fifteenth International Conference on Correlation Optics*, O. V. Angelsky, ed. (SPIE, 2021), p. 11.
21. V. Raskatla, B. P. Singh, S. Patil, V. Kumar, and R. P. Singh, "Speckle-based deep learning approach for classification of orbital angular momentum modes," J. Opt. Soc. Am. A **39**, 759–765 (2022).
22. V. Raskatla and V. Kumar, "Deep learning assisted classification of noisy Laguerre Gaussian modes," in *Frontiers in Optics + Laser Science* (OSA, 2021), paper JTu1A.16.
23. V. Raskatla, B. P. Singh, and V. Kumar, "Convolutional networks for speckle-based orbital angular momentum modes classification," Opt. Eng. **61**, 036114 (2022).
24. V. Raskatla and V. Kumar, "Deep learning assisted recognition of perfect optical vortices through astigmatic transformed speckle patterns," in *Frontiers in Optics + Laser Science* (OSA, 2022), paper JTu5A.23.
25. B. P. Singh and V. Kumar, "1D CNN empowered speckle-based non-line-of-sight communication using Hermite-Gaussian modes," in *Frontiers in Optics + Laser Science (FIO, LS)* (Optica Publishing Group, 2022), paper JW5B.56.
26. B. P. Singh and V. Kumar, "Hermite-Gaussian beams classification based on 1D speckle information using 1D convolutional neural network," in *Laser Congress (ASSL, LAC, LS&C)* (Optica Publishing Group, 2022), paper LsTu5C.3.
27. V. Raskatla, B. P. Singh, and V. Kumar, "Speckle-learned convolutional neural network for the recognition of intensity degenerate orbital angular momentum modes," Opt. Eng. **62**, 036104 (2023).
28. V. Raskatla, B. P. Singh, S. Patil, V. Kumar, and R. P. Singh, "Speckle-based recognition of OAM modes," Opt. Photon. News **51** (2022).
29. M. Naz, J. H. Shah, M. A. Khan, M. Sharif, M. Raza, and R. Damaševičius, "From ECG signals to images: a transformation based approach for deep learning," PeerJ Comput. Sci. **7**, e386 (2021).
30. M. G. Kim, H. Ko, and S. B. Pan, "A study on user recognition using 2D ECG based on ensemble of deep convolutional neural networks," J. Ambient Intell. Humaniz. Comput. **11**, 1859–1867 (2020).
31. C. B. Kristensen, K. A. Myhr, F. F. Grund, N. Vejlstrup, C. Hassager, R. Mattu, and R. Mogelvang, "A new method to quantify left ventricular mass by 2D echocardiography," Sci. Rep. **12**, 9980 (2022).
32. Á. T. Escottá, W. Beccaro, and M. A. Ramírez, "Evaluation of 1D and 2D deep convolutional neural networks for driving event recognition," Sensors **22**, 4226 (2022).
33. B. P. da Silva, B. A. D. Marques, R. B. Rodrigues, P. H. S. Ribeiro, and A. Z. Khoury, "Machine-learning recognition of light orbital-angular-momentum superpositions," Phys. Rev. A **103**, 063704 (2021).
34. P. Wang, X. Zhang, D. Fan, J. Liu, L. Sheng, Y. He, W. Xiong, Z. Huang, X. Zhou, Y. Li, and S. Chen, "Convolutional neural network-assisted optical orbital angular momentum recognition and communication," IEEE Access **7**, 162025–162035 (2019).
35. J. Anden and S. Mallat, "Deep scattering spectrum," IEEE Trans. Signal Process. **62**, 4114–4128 (2014).
36. J. Bruna and S. Mallat, "Classification with scattering operators," in *CVPR* (IEEE, 2011), pp. 1561–1566.
37. O. Yasuhiko, K. Takeuchi, H. Yamada, and Y. Ueda, "Multiple-scattering suppressive refractive index tomography for the label-free quantitative assessment of multicellular spheroids," Biomed. Opt. Express **13**, 962–967 (2022).
38. C. Li, C. Zheng, and C. Tai, "Detection of ECG characteristic points using wavelet transforms," IEEE Trans. Biomed. Eng. **42**, 21–28 (1995).
39. S. Kiranyaz, T. Ince, and M. Gabbouj, "Personalized monitoring and advance warning system for cardiac arrhythmias," Sci. Rep. **7**, 9270 (2017).
40. S. Kiranyaz, A. Gastli, L. Ben-Brahim, N. Al-Emadi, and M. Gabbouj, "Real-time fault detection and identification for MMC using 1-D convolutional neural networks," IEEE Trans. Ind. Electron. **66**, 8760–8771 (2019).
41. J. T. Ruiz, J. D. B. Pérez, and J. R. B. Blázquez, "Arrhythmia detection using convolutional neural models," in *Advances in Intelligent Systems and Computing* (Springer, 2019).